Comparison of Green-Kubo and nonequilibrium calculations of the self-diffusion constant of a Lennard-Jones fluid

Jerome J. Erpenbeck
Los Alamos National Laboratory, University of California, Los Alamos, New Mexico 87545
(Received 3 September 1986)

We apply the so-called "synthetic" nonequilibrium molecular-dynamics method to the calculation of the self-diffusion constant of a Lennard-Jones fluid at a number density of $0.85/\sigma^3$ and a temperature of $1.08\varepsilon/k_B$ (where ε and σ are the energy and length parameters of the potential and k_B is the Boltzmann constant). By comparing with the Green-Kubo calculation for the same state of the system and for the same number of particles, N, we find the latter calculation to yield more precise values of the self-diffusion constant for a given number of molecular-dynamics time steps. Even at small values of the diffusion current, a nontrivial time is needed for the nonequilibrium calculation to reach the steady state. For larger values of the driving force, the steady-state flow appears to become unstable and evidence of a secondary flow pattern is presented. The presence of these instabilities acts as a limit to the range of the driving force for which the steady-state method can be applied. With increasing N the range of stable values of the diffusion current density decreases. For the Green-Kubo calculations, the N dependence of the self-diffusion constant is found to be anomalous for $N=108$, with the $1/N$ dependence only exhibited for at least 500 particles. The nonequilibrium results, while approximately independent of N for 108 and 500 particles, are found to have a similar anomalous N dependence when we extend the calculations to 1372 particles, thereby bringing the Green-Kubo and nonequilibrium results into agreement in the large-system limit.

I. INTRODUCTION

The evaluation of transport coefficients for dense fluids, beyond the level of approximate theory, relies on the use of the numerical methods of Monte Carlo and molecular dynamics (MD). In particular, the molecular-dynamics method has been applied to the transport coefficient calculation nearly from its inception.[1] Early calculations of transport coefficients were based, for the most part, on the Green-Kubo theory,[2,3] whereby any transport coefficient μ is obtained from an appropriate time-correlation function $\rho_\mu(t)$, through

$$\mu = c_\mu \int_0^\infty dt\, \rho_\mu(t) , \tag{1}$$

in which $\rho_\mu(t)$ is an appropriate time-correlation function, viz.,

$$\begin{aligned} \rho_\mu(t) &= \mathrm{tlim}\, \rho_\mu(t;N) , \\ \rho_\mu(t;N) &= \langle J_\mu(0) J_\mu(t) \rangle , \end{aligned} \tag{2}$$

in which tlim denotes the thermodynamic limit of large system size, the $\langle\ \rangle$ denote an average over an equilibrium ensemble, and the microscopic current $J_\mu(t)$ is a known function of the phase $x^N(t)=(r^N(t),v^N(t))$ (in which r^N and v^N are the position and velocity vectors of the N particles in the system, respectively, in dN-dimensional space, the dimensionality d here being either 2 or 3), and c_μ is a constant. The Green-Kubo method depends on the evaluation of the microscopic current at a time t subsequent to an initial time 0 by the application of the molecular-dynamics method to generate an N-particle trajectory $x^N(t)$, with the ensemble average being either replaced by a time average[1] over "time origins" equally spaced (in time) along the trajectory, or evaluated by a combination of Monte Carlo and molecular-dynamics averaging,[4] using a number of trajectories whose initial phases are selected by Monte Carlo from an equilibrium ensemble.

One of the most important results from the application of these ideas to the calculation of transport coefficients was the discovery of the slow decay of time-correlation functions, which has been termed the "long-time tail." For self-diffusion, it was found that at long times[5-7]

$$\rho_D(t) \sim \alpha_D (t/t_0)^{-d/2} , \tag{3}$$

at least for hard "spheres" of dimension d (=2 or 3) at fluid densities. The result Eq. (3) has been obtained theoretically as well.[8,9]

One consequence of this slow decay is that the full values of the transport coefficients obtained through Eq. (1) are achieved rather more slowly than predicted, say, by the Boltzmann-Enskog theory. Furthermore, because of this need to include contributions to the integral in Eq. (1) out to large times, to obtain precise values for μ it is necessary either to compute to rather late times t or to include the long-time contribution theoretically. If numerical calculation is used at long times, then it is found that finite-system effects become relatively large for values of t greater than the time needed for an acoustic wave to traverse the system. This effect arises from the propagation of the microscopic fluctuations in the hydrodynamic variables throughout the length of the system.[6] Thus, the numerical study of long times necessitates the study of large systems. Based strictly on numerical evaluation,

without the benefit of the theoretical results for long-time tails, then, the precise evaluation of transport coefficients can be difficult.

This difficulty is at least partially responsible for the invention of a second path to numerical evaluation of transport coefficients. Early versions of nonequilibrium molecular dynamics sought to mimic laboratory experiment,[10–12] using the computer to impose nonequilibrium boundary conditions on a system of N interacting particles. By driving the system to a stationary (or at least approximately stationary) flow, one hopes to evaluate the transport coefficient as an appropriate ratio of flux to gradient, much in the manner of laboratory experiment. Because one obtains nonequilibrium through the use of boundary conditions, these methods are referred to as "boundary-driven" NEMD (nonequilibrium MD). One attractive feature of such calculations is the possibility of studying the nonequilibrium system in great detail, both with respect to spatial and temporal effects. Unfortunately, whether of necessity or of convenience, the driving forces in such calculations were very large, when compared with those which are found in the laboratory. A twofold effect of the excessive magnitude of the driving forces were (1) the need to extract energy from the system such that a steady state will be achieved, and (2) the observation of a significant dependence of the transport coefficient on the gradient of the appropriate intensive variable which characterizes the transport process under study. A third effect, which is not so commonly recognized, is the slow approach to the steady state which is particularly important when the gradients are large.

The principal problem recognized at the outset in the application of boundary-driven NEMD arises from the inevitable inhomogeneity of such systems whereby the thermodynamic state changes throughout the system. While thermodynamic inhomogeneity is, of course, inherent in experiments on transport processes, the difference between the NEMD and actual experiment is one of scale. In a spatial region sufficiently small compared to the magnitude of the gradients that one can sensibly define a thermodynamic state, there might typically be very few particles, far fewer than the number of particles typically used in molecular dynamics. As a result, one frequently is forced to deal with difficult problems of data analysis arising from the sensitivity of the calculated transport coefficient to the spatial scale over which state variables and currents are defined.

More recently, a "synthetic" approach to NEMD has been devised,[13,14] the aim of which is to deal with a homogeneous nonequilibrium system through the addition of homogeneous external forces. Using an approach based in part on the linear-response approach to the Green-Kubo formulas, it has been possible to obtain external forces appropriate to any of a variety of transport effects which lead to a nonequilibrium current without the attendant gradient, the current instead being driven by the external forces. Moreover, by the inclusion of additional external forces to cool the system homogeneously, one has a system which would be expected to approach (with time) a steady state. One calculates the current as a function of the magnitude of the driving force to obtain a nonequilibrium transport coefficient. By considering the limit of vanishing external force, one expects to recover the true (long-wavelength, small gradient) transport coefficient. It has been widely suggested[15,16] that these synthetic NEMD calculations are vastly superior in calculational efficiency to previous methods because of (1) an apparent improvement in the statistical properties of the observation of the steady-state current and (2) the suppression of the large N dependence of the boundary-driven methods through the homogeneity of the system. Furthermore, it is widely believed that the N dependence of these NEMD methods is vastly improved compared to the Green-Kubo method. Indeed, it is commonly assumed that the transport coefficients obtained in these calculations for as few as 108 particles are essentially equal to the infinite-system values.

An additional question raised by these synthetic NEMD methods concerns their significance away from equilibrium. One might reasonably ask whether these calculations are meaningful at values of the driving force for which the observed hydrodynamic currents are no longer in the linear-law (i.e., the so-called "Newtonian") regime. As far as we are aware, there is no theoretical arguments to connect, for example, the dependence of the mutual diffusion coefficient on the diffusion current in a synthetic NEMD calculation with that for a laboratory experiment in which one would typically have control of certain boundary conditions.

It is our purpose here to examine the claims of the synthetic method by comparing it with the supposedly "out-of-date" Green-Kubo method for the case of self-diffusion. Because of the simplicity of the self-diffusion process, it would seem to be a reasonable first test for the method. Moreover, because there are no non-Newtonian effects associated with self-diffusion,[17] it provides a test for the NEMD method away from equilibrium for a case for which a great deal is known.

Inasmuch as very extensive studies of self-diffusion have been made for the hard-sphere potential,[7] it would appear most natural to make such a comparison for hard spheres. Nonetheless the external forces introduced in the NEMD cause the particle trajectories to no longer follow straight lines between collisions and the computational advantage normally associated with the hard-sphere potential is thereby lost. Therefore, we use a Lennard-Jones potential, truncated at a finite range as described in Sec. II. Also in Sec. II, we detail the nature of our system and give the expressions for the diffusion forces as well as the forces which maintain the temperature in the nonequilibrium system. In Sec. III, we describe some details of our numerical methods, both for the Green-Kubo calculation and for the NEMD calculation. In Sec. IV we discuss the results, leaving their interpretation to a final Sec. V.

II. MOLECULAR DYNAMICS OF SELF-DIFFUSION

A. Dynamical system

We consider an equimolar, two-component system of N particles, each of mass m, interacting through a pairwise-additive potential $u(r)$, subject to the usual periodic boundary conditions. The Newtonian equations of

motion are

$$m\ddot{x}_i = F_{xi} ,$$
$$m\ddot{y}_i = F_{yi} , \tag{4}$$
$$m\ddot{z}_i = F_{zi} ,$$

in which $\mathbf{F}_i$ is the force on particle i arising from the $N-1$ other particles (as well as the "image" particles in periodic boundary conditions).

For the interparticle potential, we use the Lennard-Jones potential, truncated via a cubic "spline," suggested by Holian and Evans,[18] which vanishes at the cutoff distance r_m with vanishing first and second derivatives,

$$u(r) = \begin{cases} \phi(r), & r < r_c \\ a(r-r_m)^2 + b(r-r_m)^3, & r_c < r < r_m \\ 0, & r_m < r \end{cases} \tag{5}$$

where $\phi(r)$ is the Lennard-Jones (LJ) potential,

$$\phi(r) = 4\varepsilon \left[\left(\frac{\sigma}{r} \right)^{12} - \left(\frac{\sigma}{r} \right)^{6} \right] .$$

The parameter r_c is defined to be the point of maximum attraction,

$$r_c = (\tfrac{26}{7})^{1/6}\sigma \tag{6}$$

of the LJ potential. The parameters a, b, and r_m of the cubic spline are defined by requiring that $u(r)$ and its first and second derivatives be continuous at r_c, whence

$$r_c - r_m = 3\phi_0/2\phi_1 ,$$
$$a = \phi_1/(r_c - r_m) , \tag{7}$$
$$b = -\phi_1/3(r_c - r_m)^2 ,$$

in which ϕ_n is the nth derivative of the LJ potential $\phi(r)$, at $r = r_c$.

B. Green-Kubo method

The Green-Kubo formula, Eqs. (1) and (2), for the self-diffusion constant requires

$$J_D(t) = u_{xi}(t) ,$$
$$\mathbf{u}_i(t) = \mathbf{v}_i(t) - \bar{\mathbf{v}} , \tag{8}$$
$$\bar{\mathbf{v}} = \sum_{i=1}^{N} \mathbf{v}_i/N ,$$
$$c_D = 1 ,$$

in which i denotes the index of any particle. The calculation of D by the Green-Kubo method has been detailed for hard spheres and disks,[6,7] and we follow a very similar approach here. The ensemble average to be evaluated, Eq. (2), is estimated using the Monte Carlo (MC) method, now in the canonical ensemble rather than the microcanonical ensemble employed in the hard-sphere study. The Metropolis technique[19] yields a sequence of P configurations $\{r_p^N;\ p = 1,2,\ldots,P\}$. A corresponding sequence of N-particle velocities $\{v_p^N;\ p = 1,2,\ldots,P\}$ are chosen randomly from the Maxwell-Boltzmann distribution using the Box-Muller method.[20] We use molecular dynamics to generate from each such phase point a trajectory $\{x_p^N(t);\ 0 \le t \le t_f\}$, in which t_f is some fixed final time, chosen to be much larger than the values of t of interest.

A time average of any two-point function of interest,

$$H(t;\tau) = f(x^N(\tau))g(x^N(\tau+t)) ,$$

is obtained by averaging over a sequence of Q "time origins" $\{t_q;\ q = 1,2,\ldots,Q\}$,

$$\bar{H}_p(t) = \frac{1}{Q}\sum_{q=1}^{Q} f(x_p^N(t_q))g(x_p^N(t_q+t)) ,$$

in which the t_q are equispaced over $(0,t_f)$,

$$t_q = (q-1)t_f/Q .$$

We obtain averages and statistical uncertainties from the P values of $\bar{H}_p(t)$.

In the current calculations, as distinguished from the earlier hard-sphere calculations,[7] the MC sequence x_p^N differs from the normal Metropolis random walk in that the MC configuration r_{p+1}^N is obtained by the usual sequence of trial displacements starting from $r_p^N(t_f)$ rather than from $r_p^N(0)$. Because energy is conserved dynamically, the probabilities of the states $x_p^N(0)$ and $x_p^N(t_f)$ are the same in the canonical ensemble, so that this change does not appear to affect the validity of the Metropolis method (although a detailed proof is not given here).

Our Green-Kubo calculations will concentrate on the integral of the velocity autocorrelation function,

$$D(t;N) = \int_0^t ds\, \rho_D(s;N)$$
$$= \langle u_{xi}(0)\Delta R_{xi}(t) \rangle ,$$
$$\mathbf{R}_i(t) = \mathbf{r}_i(t) - \bar{\mathbf{v}}t , \tag{9}$$

in which $\Delta\mathbf{R}_i(t) = \mathbf{R}_i(t) - \mathbf{R}_i(0)$ is the displacement of the ith particle in the center-of-mass frame of reference.

C. Nonequilibrium molecular-dynamics method

For the NEMD calculation, a number of different methods have been proposed. The synthetic method has been described for self-diffusion by Evans *et al.*,[13,14] and applied to the Lennard-Jones potential. Here we implement the constant-diffusion-current variant (i.e., the so-called "Gaussian algorithm") of it. The particles, previously regarded as identical, are now assigned a color label c_i which will have significance only for the NEMD calculations; for i even, $c_i = 1$ and for i odd, $c_i = -1$. While we could equally well consider cases of varying concentrations of the two species, our interest centers on the self-diffusion process, so that effects arising from the differences in the number of particles of each species will not be important and a symmetric specification of the system therefore seems rather natural. The equations of motion are now written in the non-Newtonian form,[13,14]

$$m\ddot{x}_i = F_{xi} - \lambda_d c_i ,$$
$$m\ddot{y}_i = F_{yi} - \lambda_s m\dot{y}_i , \tag{10}$$
$$m\ddot{z}_i = F_{zi} - \lambda_s m\dot{z}_i ,$$

in which the constraint of fixed (i.e., time-independent) diffusion current,

$$I_D=\sum_{i=1}^{N} c_i v_{xi} , \tag{11}$$

yields the driving force

$$\lambda_d=\frac{\sum_{i=1}^{N} c_i F_{xi}}{N} . \tag{12}$$

The constraint of fixed transverse kinetic energy,

$$E_t=\tfrac{1}{2}\sum_{i=1}^{N} m(v_{yi}^2+v_{zi}^2) , \tag{13}$$

yields the "thermostat" parameter

$$\lambda_s=\frac{\frac{1}{2}\sum_{i=1}^{N}(v_{yi}F_{yi}+v_{zi}F_{zi})}{E_t} . \tag{14}$$

It is possible to fix the total kinetic energy of the system using a modification of these equations, but we have not done so in this study.

The values of the diffusion current I_D, and the transverse kinetic energy E_t, for a trajectory are determined by their initial values. To impose specified values of these parameters we have simply modified the initial velocities $\mathbf{v}_i$ produced by the Monte Carlo procedure (as described above for the Green-Kubo calculation) by calculating new velocities,

$$\begin{aligned} v'_{xi}&=v_{xi}+\delta_i , \\ v'_{yi}&=\alpha(v_{yi}-\bar{v}_y) , \\ v'_{zi}&=\alpha(v_{zi}-\bar{v}_z) , \end{aligned} \tag{15}$$

with

$$\begin{aligned} \delta_i&=(c_i I_D-2L_i)/N , \\ L_{2i}&=\sum_{j=1}^{N/2} v_{x,2j} , \\ L_{2i+1}&=\sum_{j=1}^{N/2} v_{x,2j-1} , \\ \alpha^2&=\frac{2Nk_BT}{m}\left[\sum_{i=1}^{N}(v_{yi}^2+v_{zi}^2)-N(\bar{v}_y^2+\bar{v}_z^2)\right]^{-1} . \end{aligned} \tag{16}$$

The total linear momentum is readily seen to vanish for the primed velocities. Further, it should be noted the total linear momentum remains a constant of the motion in the presence of the external forces, although the total energy now fluctuates in time.

It should also be observed that the equilibrium molecular-dynamics calculation trajectory is not simply the NEMD trajectory with the I_D set at zero. Indeed, in ordinary molecular dynamics both the diffusion current and the transverse kinetic energy fluctuate in time about their equilibrium values. While the Green-Kubo calculation can be done using the constrained equations of motion, for the most part we chose the more conventional method.

The principal aim in imposing the constraint of fixed kinetic energy in the nonequilibrium calculation is to permit the system to achieve a steady state at long times. There is no proof that a steady flow will, in fact, be achieved, but from the hydrodynamic point of view, one would certainly expect that it would.

To calculate the self-diffusion constant using the NEMD method, we follow Evans *et al.*[13,14] to obtain two distinct values of D,

$$D_d=\frac{(N-1)k_BTI_D^2}{N^2\langle P_d\rangle_{\rm ne}} , \tag{17}$$

$$D_s=-\frac{(N-1)k_BTI_D^2}{N^2\langle P_s\rangle_{\rm ne}} , \tag{18}$$

in which $\langle\ \rangle_{\rm ne}$ denotes the long-time (assumed) steady-state time average, and the power functions (viz., power expended on the system by the external forces) are given by

$$\begin{aligned} P_d&=\lambda_d I_D , \\ P_s&=-2\lambda_s E_t . \end{aligned} \tag{19}$$

Values of D for several values of the diffusion current I_D were reported by Evans *et al.*[13,14] for the LJ potential (differing from ours in the absence of the cubic spline), both for the "Gaussian" method, as described here, and the "Hamiltonian" method. Only small differences between the two sets of results were visible. Because these authors did not report the statistical precision of their results and because their calculations were not extensive, only a rather superficial comparison with the Green-Kubo results of Levesque and Verlet,[21] was possible. Our principle aim here is to extend these calculations in such a way that questions of validity and merit can be unequivocally decided.

III. NUMERICAL TECHNIQUES

In this section, we describe the calculations performed both for the equilibrium and nonequilibrium methods. In addition to defining the reduced variables which are used to define the calculations and the results, we also describe the statistical treatment of the data.

A. Reduced variables

The state of the system is described through the reduced density, temperature, and diffusion current density,

$$\begin{aligned} \hat{n}&=N\sigma^3/V , \\ \hat{T}&=k_BT/\varepsilon , \\ \hat{J}_D&=\sigma^3(m/\varepsilon)^{1/2}I_D/V , \end{aligned} \tag{20}$$

which correspond to our choice of m, σ, and t_0,

$$t_0=\sigma\sqrt{m/\varepsilon} , \tag{21}$$

for our units of mass, length, and time, respectively. In general, we denote reduced variables by the use of an overhanging caret, but the reader is forewarned to distin-

guish the symbol $\hat{\mathbf{e}}_a$ ($a=x$, y, or z) which we use for the unit vector in the direction of the a axis.

B. Finite-difference method

A number of finite-difference methods for integrating the equations of motion have been reviewed by Berne and Harp.[22] We have used the Verlet[23] central-difference technique, in which the (reduced) position of particle i, determined at integral time steps, and the (reduced) velocity of particle i, determined at half time steps, are given by the relations

$$\hat{\mathbf{R}}_{i,n+1}=\hat{\mathbf{R}}_{i,n}+\hat{h}\hat{\mathbf{u}}_{i,n+1/2}\ , \tag{22}$$

$$\hat{\mathbf{u}}_{i,n+1/2}=\hat{\mathbf{u}}_{i,n-1/2}+\hat{h}\hat{\mathbf{G}}_{i,n}\ , \tag{23}$$

where the total force is

$$\hat{\mathbf{G}}_{i,n}=\hat{\mathbf{F}}_{i,n}-c_i\hat{\mathbf{e}}_x(\hat{\lambda}_d)_n-(\hat{u}_{yi,n}\hat{\mathbf{e}}_y+\hat{u}_{zi,n}\hat{\mathbf{e}}_z)(\hat{\lambda}_s)_n \tag{24}$$

(where h denotes the time step, $\hat{\mathbf{e}}_\alpha$ is the unit vector along the α axis, and the n subscripts on, for example, $\hat{\mathbf{R}}$, $\hat{\mathbf{u}}$, and $\hat{\mathbf{G}}$ specify the time-step index). This method was discussed by Berne and Harp,[22] and was chosen here because of its simplicity and the favorable experience reported by Holian and Evans[18] as well as others.

In Eq. (24) the $\hat{\mathbf{F}}_{i,n}$ depends only on the positions $\hat{\mathbf{R}}_n^N$, so that for our Green-Kubo calculations, in which the λ's vanish, Eqs. (22)—(24) provide an explicit determination of the finite-difference trajectory. For the NEMD equations of motion, the "driving" term λ_d is also dependent only on the positions, as is seen from Eq. (12), but the thermostat terms depend on u_n^N; the latter quantity is only computed at half time steps, as seen from Eq. (23). In order to compute λ_s consistently, we substitute Eq. (23) for $\hat{\mathbf{u}}_{i,n+1/2}$ into the central-difference approximation,

$$\hat{\mathbf{u}}_{i,n}=(\hat{\mathbf{u}}_{i,n+1/2}+\hat{\mathbf{u}}_{i,n-1/2})/2\ . \tag{25}$$

Combining with Eqs. (24) and (14), we can solve for the finite-difference approximation for λ_s:

$$\begin{aligned}
&(\hat{\lambda}_s)_n=g_n/(1-\hat{h}g_n/2)\ ,\\
&g_n=\frac{A_n+\hat{h}B_n/2}{C_n+\hat{h}A_n+\hat{h}^2B_n/4}\ ,\\
&A_n=\sum_{i=1}^{N}(\hat{u}_{yi,n-1/2}\hat{F}_{yi,n}+\hat{u}_{zi,n-1/2}\hat{F}_{zi,n})\ ,\\
&B_n=\sum_{i=1}^{N}(\hat{F}_{yi,n}^2+\hat{F}_{zi,n}^2)\ ,\\
&C_n=\sum_{i=1}^{N}(\hat{u}_{yi,n-1/2}^2+\hat{u}_{zi,n-1/2}^2)\ .
\end{aligned} \tag{26}$$

Using this expression for $\hat{\lambda}_s$, the desired conservation of the transverse kinetic energy is achieved to reasonably high precision, viz., to about two parts in 10^6 in the present calculations.

C. Calculation of Green-Kubo diffusion constant

We present our results for the diffusion constant in reduced units,

$$\hat{D}=(m/\varepsilon)^{1/2}D/\sigma\ . \tag{27}$$

In the Green-Kubo calculations, we base our results on the "time-dependent" diffusion constant, Eq. (9), which yields the reduced quantity

$$\hat{D}(\hat{t};N)=\langle\hat{u}_{xi}(0)\Delta\hat{R}_{xi}(\hat{t})\rangle\ . \tag{28}$$

There is, of course, some difficulty in deciding how large $\hat{t}$ should be taken in order that $\hat{D}(\hat{t};N)$ has essentially attained the limiting value,

$$\hat{D}(N)=\lim_{\hat{t}\to\infty}\hat{D}(\hat{t};N)\ . \tag{29}$$

In the present calculations, we evaluate $\hat{D}(\hat{t}^*;N)$ with $\hat{t}^*$ chosen sufficiently large that the velocity autocorrelation function is in reasonable agreement with the theoretical long-time tail, Eq. (3), for $t\sim\hat{t}^*t_0$, at least for sufficiently large values of N. We then combine the extrapolated,

$$\hat{D}(\hat{t}^*)=\lim_{N\to\infty}\hat{D}(\hat{t}^*;N)\ ,$$

with the theoretical long-time tail contribution to obtain our final estimate for $\hat{D}$.

The statistical treatment of the time-correlation function data has been discussed in some detail for the hard-sphere and hard-disk calculations[6,7] and is not repeated here. Since we are for the most part simply concerned with the evaluation of $\hat{D}(\hat{t};N)$, we can use standard statistical methods to treat the sequence of values of the time-averaged quantity, with one value provided by each of the trajectories. The only complication in the present calculations occurs in certain instances in which the first configuration selected by our Monte Carlo procedure has not moved sufficiently far from the face-centered-cubic lattice which is used as the initial configuration for each realization. In such instances we have simply discarded the observations for the first trajectory. In no instance did the solidlike configuration persist beyond the first trajectory.

D. NEMD calculations

1. *Diffusion constant*

In the NEMD calculations, one expects that, even though the diffusion current is fixed at the outset, a nontrivial transient should be presented as the system approaches a steady state. It is well known that the long-wavelength components of the hydrodynamic variables will decay quite slowly. Typically this slow decay makes it necessary to wait some time before the observations will characterize the steady state. In our program, therefore, observations are not made for the first Γ times steps of the trajectory, although in some cases a value $\Gamma=0$ is used. At succeeding time steps, the quantities $\hat{P}_s$ and $\hat{P}_d$ are computed as well as a number of other quantities, including the kinetic and potential energies; other quantities are computed at less frequent intervals, as described below. All the observed quantities are then "coarse

grained" over 1000 time-step intervals, e.g.,

$$\hat{P}_{dj}=(\tfrac{1}{1000})\sum_{i=1000(j-1)+1}^{1000j}\hat{P}_d(ih)\ ,$$

and the coarse-grained observations $\hat{P}_{dj}$ saved for subsequent statistical analysis. At the time of data reduction, if a transient is still seen, further observations can be omitted; we report the total number of time steps Θ which are ignored in averaging our values of the power functions and thence the reported values of $\hat{D}$.

Because our 1000-step coarse-graining interval is small compared to macroscopic times, successive values of the observations are correlated, reflecting the slow decay of fluctuations in the system. In order to obtain quantities which appear to be normally distributed (enabling the application of the standard statistical estimates of precision), these values are usually further coarse grained; therefore, we report the overall number Ω of coarse-graining time steps used in computing the average values of P_s and P_d and their associated statistical precision. We choose Ω sufficiently large that the individual values appear uncorrelated. The suitability of Ω can be judged by applying a number of the standard tests[24] for a normal distribution. Here we routinely compute the mean-square successive ratio, the skew, the excess, as well as several of the "runs" tests to ascertain that Ω is sufficiently large.

In Fig. 1 we illustrate these points by presenting the "control chart" for the coarse-grained average of the reduced P_d for a NEMD calculation for 500 particles for the state $\hat{T}=1.08$, $\hat{n}=0.85$, $\hat{J}_x=0.03$. The time step $\hat{h}=0.002$ is typical of those reported below. In this case, Γ is 0 so that the results for the entire trajectory are included in the figure. The values in the figure represent averages $\hat{P}_{dj}$ over successive 1000-step intervals, plotted against the "index" j of the observation, simply labeled "observation." The presence of an initial transient is strongly indicated. After roughly five time intervals, it would appear that a steady state has been achieved, so that we take $\Theta=5000$. The similar plot for the temperature of the system (obtained from the total kinetic energy) supports this conclusion. The coarse-graining interval $\Omega=1000$ used in this figure might appear to be sufficient so that successive values of the dependent variable are uncorrelated. This conclusion is contradicted by application of the statistical tests for the points having index greater than 5 in the figure. We require a coarse-graining interval $\Omega=5000$ to suppress the serial correlation of these data.

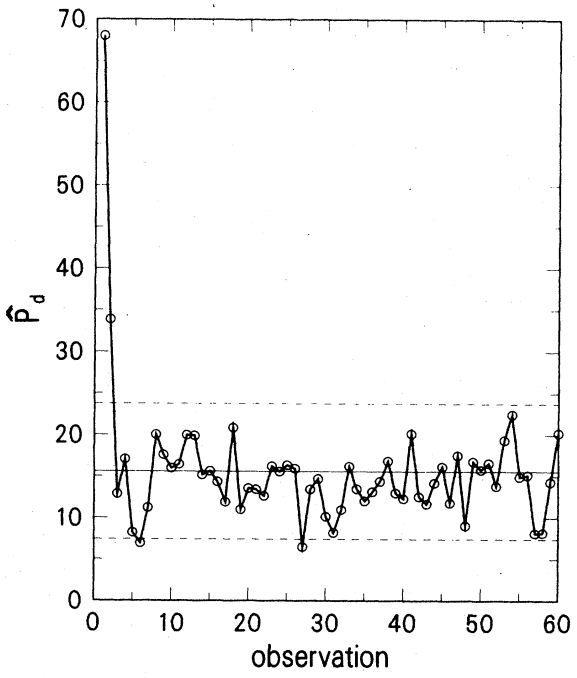

FIG. 1. Control chart for the reduced power function $\hat{P}_d$ observed in a NEMD calculation of the self-diffusion constant for a system of $N=500$ particles at a reduced diffusion current $\hat{J}_x=0.03$, a reduced temperature $\hat{T}=1.08$, and a reduced number density $\hat{n}=0.85$, showing the decay of a transient as the system approaches an apparent steady state of constant diffusion current. The abscissa is the sequence number of the observations, each of which consists of a coarse-grained average over a 1000 time-step interval. The points are connected with a solid line as a guide to the sequence of the observations. The solid horizontal line marks the mean of the displayed data and the dashed lines mark one standard deviation of the population above and below the mean.

2. *Correlation functions*

In addition to the statistical tests, we also make an attempt to observe large hydrodynamic fluctuations by calculating the structure factors, viz., the Fourier components of the pair correlation functions,

$$g_{\alpha\beta}(\mathbf{s}_1,\mathbf{s}_2)=n_\alpha^{-1}n_\beta^{-1}\left\langle\sum_{\nu}\sum_{i\in C_\alpha}\sum_{j\in C_\beta}{}'\,\delta(\mathbf{r}_i-\mathbf{s}_i)\delta(L\boldsymbol{\nu}+\mathbf{r}_j-\mathbf{s}_2)\right\rangle_{\rm ne}\ , \tag{30}$$

in which the ν sum denotes a sum over all triples of signed integers, L denotes the length of the system which is taken to be cubic, the subscripts α and β range over indices, 0 and 1, of the two "species," C_0 is the set of odd particle indices, C_1 is the set of even particle indices, and the prime on the j sum indicates that the term $j=i$ is to be excluded for $\nu=(0,0,0)$. Because the system is homogeneous, $g_{\alpha\beta}$ is a function only of $\mathbf{s}=\mathbf{s}_1-\mathbf{s}_2$. Therefore,

writing the Fourier transform,

$$S_{\alpha\beta}(\mathbf{k})=V^{-1}\int_V d\mathbf{s}\exp(2\pi i\mathbf{k}\cdot\mathbf{s}/L)g_{\alpha\beta}(0,\mathbf{s}) \tag{31}$$

(in which $\mathbf{k}$ is a three-vector of signed integers), we obtain

$$S_{\alpha\beta}(\mathbf{k})=N_\alpha^{-1}N_\beta^{-1}\left\langle \sum_{i\in C_\alpha}\sum_{j\in C_\beta}{}' \exp[2\pi i\mathbf{k}\cdot(\mathbf{r}_i-\mathbf{r}_j)/L]\right\rangle_{\text{ne}} . \tag{32}$$

While in general $S_{\alpha\beta}$ is not isotropic in $\mathbf{k}$, for the equilibrium system, it is expected to be nearly isotropic except for very small systems, i.e., values of N, and additionally independent of the species labels. For the nonequilibrium case, we expect a dependence on direction to be important, even for large system sizes. For this reason we compute the six quantities

$$S_{\alpha\beta}^{(a)}(k)=S_{\alpha\beta}(k\hat{\mathbf{e}}_a) , \tag{33}$$

for $a=x,y,z$ and $\alpha=0$, $\beta=0,1$. Fluctuations in these quantities, especially the long-wavelength components (e.g., $k=1$), are expected to decay quite slowly, inasmuch as these represent two-particle density fluctuations. When coarse grained over a sufficiently large number Ω_s of time steps, these values should also be distributed approximately normally and the presence of transients should then be indicated by a residual dependence on the time.

Of particular interest is a closely related quantity, the color density,

$$\begin{aligned} F_{\mathbf{k}}&=n^{-2}\langle n_{\mathbf{k}}n_{-\mathbf{k}}\rangle_{\text{ne}} ,\\ n_{\mathbf{k}}&=V^{-1}\int_V d\mathbf{s}\exp(2\pi\mathbf{k}\cdot\mathbf{s}/L)n(\mathbf{s}) ,\\ n(\mathbf{s})&=\sum_{\nu}\sum_{i=1}^{N} c_i\delta(L\boldsymbol{\nu}+\mathbf{r}_i-\mathbf{s}) . \end{aligned} \tag{34}$$

For the (equilibrium) N-V-T ensemble, it is readily found that, to order $1/N$,

$$F_{\mathbf{k}}^{(\text{eq})}=1/N ,$$

but, in general, we obtain, using Eqs. (32) and (33),

$$F_{k\hat{\mathbf{e}}_a}=\frac{1}{2}\left[\frac{2}{N}+S_{00}^{(a)}(k)-S_{01}^{(a)}(k)\right] . \tag{35}$$

It is expected that the magnitude of these quantities should not differ greatly from their equilibrium value, except when the structure of the fluid changes dramatically as, for example, at the onset of a secondary flow when the homogeneous flow becomes unstable. In particular, we compute the average of the transverse components,

$$F(k)=(F_{k\hat{\mathbf{e}}_y}+F_{k\hat{\mathbf{e}}_z})/2 , \tag{36}$$

for the longest wavelengths which the system can contain, viz., $k=1$.

A control chart for $S_{00}^{(x)}(1)$ is given in Fig. 2 for a 500-particle system at the same density, temperature, and current density as in Fig. 1. In this case, however, the observations are not made at each time step but at every twentieth step; the individual points in Fig. 2 represent averages over 50 observations spaced at 20 time-step intervals. This presents quite a different picture of the approach to the steady state from Fig. 1. One might, for example, easily conclude that the first 70 000 time steps for this system represent the approach to steady conditions and that the fluctuations themselves are much longer lived; a choice of $\Omega_s=20\,000$ might seem reasonable. However, when we analyze the Fig. 2 data in this way, we are left with very few coarse-grained observations; as a result it is difficult to conclude with much confidence whether the system has actually reached the steady state with respect to $S_{00}^{(x)}(1)$.

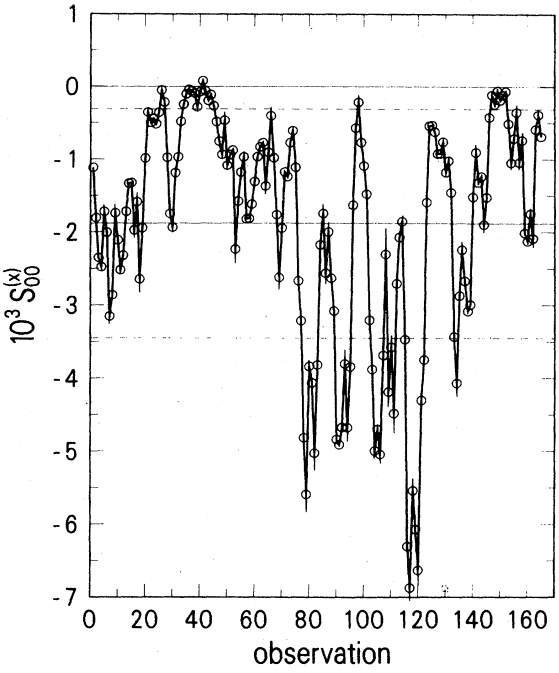

FIG. 2. Control chart for the static structure factor $\hat{S}_{00}^{(x)}(k)$ for $k=1$ for an NEMD calculation similar to that of Fig. 1, showing the existence of large, slowly decaying fluctuations as well as a strongly coherent time dependence. See Fig. 1 for details.

The fact that the two-particle distributions exhibit long-lived fluctuations, as seen here, does not require that our calculation of averages for the power functions (and hence for the diffusion constant) be delayed until such long times. Indeed, we would naturally expect that higher-order distribution functions will approach steady-state values more slowly than low-order distributions. Thus, we use the control charts and the associated statistical tests as previously described to judge when P_d, for example, appears to have reached the steady state, to a large measure independently of the behavior displayed in the control charts for the $S_{\alpha\beta}^{(a)}$.

IV. RESULTS

We have made rather extensive calculations for a single state point, namely, the same state treated by Evans *et al.*,[13] $\hat{T}=1.08$, $\hat{n}=0.85$, for systems of 108, 500, and 1372 particles. One calculation for $N=864$ has also been made, for reasons which will become apparent. Our po-

tential energy differs from that of Evans *et al.* for separations greater than the crossover r_c, Eq. (6), because of our use of the cubic spline for $r_c < r < r_m$. A graphical comparison of the spline with the full LJ potential was given by Holian and Evans.[18] Our value of the cutoff distance is $r_m \sim 1.74\sigma$, compared with 2.5σ used by Evans *et al.* As we shall show, there appears to be no readily discernible effect of these differences.

A. Green-Kubo results

In Table I, we list the relevant parameters and results for the four Green-Kubo calculations, including the time-origin spacing ω (in time steps) and the greatest number θ of time steps for which the time-correlation functions are computed. The values of the self-diffusion constant listed in the table are the values of $\hat{D}(\theta\hat{h};N)$, which do not include the contributions associated with the long-time tail of the VACF. This can be seen from Fig. 3 which shows the reduced autocorrelation function (VACF),

$$\hat{\rho}_D(\hat{t};N)=(m/\varepsilon)\langle u_{xi}(0)u_{xi}(t_0\hat{t})\rangle \tag{37}$$

as a function of time at relatively late times, i.e., beyond the known, negative, minimum of the function,[21] for $N=108$, 500, and 1372. Thus, the values of $\hat{D}(\theta\hat{h};N)$ given in the table include contributions only a little beyond the point at which the VACF has become positive, at which point the long-time tail might be expected to begin.

We observe that the values of $\hat{D}(\theta\hat{h};N)$, given in Table I show the existence of an anomalous dependence on the number of particles for $N=108$, in that the expected approach to the infinite-system limit as a function linear in $1/N$ is not evidenced at $N=108$. Instead, this contribution to the diffusion constant (as a function of N) has a maximum between $N=108$ and 1372. Similarly the compressibility factor,

$$Z_N(n,T)=pV/Nk_BT\ , \tag{38}$$

also tabulated in the table, exhibits a maximum. The equations of state of the hard-disk[25] and the hard-sphere[26] fluids are known to have similar anomalies in their N dependence at high fluid densities. For transport properties, Hoover *et al.*[27] presented Green-Kubo results for the shear viscosity of the Lennard-Jones fluid at $\hat{n}=0.8442$ and $\hat{T}=0.7$, based on calculations from a number of different sources, indicating a possible minimum in the viscosity coefficient between $N=108$ and $N=500$.

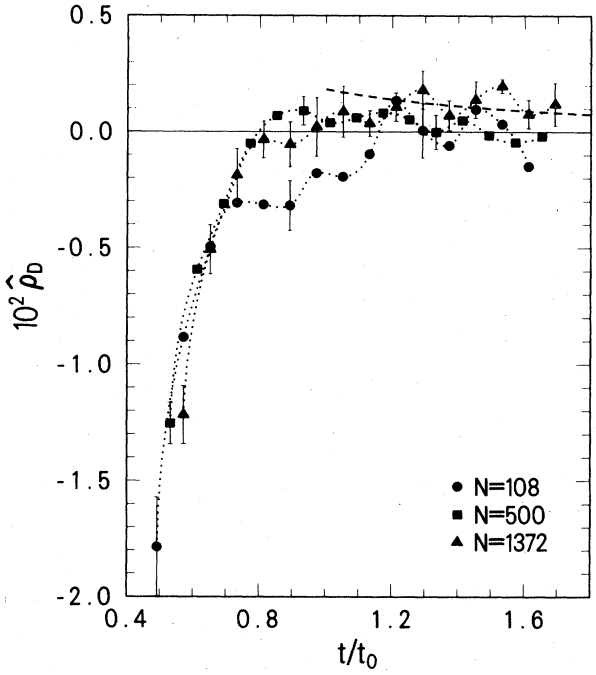

FIG. 3. Reduced velocity autocorrelation function in the N-V-T ensemble as a function of reduced time (units t_0) for the Lennard-Jones fluid at a reduced number density $\hat{n}=0.85$ and a reduced temperature $\hat{T}=1.08$, for systems of 108 (circles), 500 (squares), and 1372 (triangles) particles. The dashed curve is the theoretical prediction for the long-time tail for the velocity autocorrelation function. The dotted curves join the points and are added as a guide to the eye.

While the source of the upturn in the viscosity with decreasing N has not been discussed (indeed, it appears to be viewed with suspicion by many workers), for the present case of self-diffusion, it is clear that the anomaly arises at early times for which we find the VACF for the three different system sizes can be brought into approximate coincidence by applying an appropriate scaling of the time.

TABLE I. Parameters and results for the Green-Kubo calculations of the self-diffusion constant for the Lennard-Jones fluid in the N-V-T ensemble at a reduced density $\hat{n}=0.85$ and reduced temperature $\hat{T}=1.08$. N is the number of particles, P is the number of trajectories, h is the integration time step, t_f is the final time for each trajectory, ω is the time steps per time origin, θ is the maximum number of time steps for which time-correlation functions are computed, N_t is the total number of time steps, ν is the number of degrees of freedom for the averages, pV/Nk_BT is the compressibility factor, $\hat{D}$ is the reduced self-diffusion constant, and v_0 is a normalized statistical error estimate. The statistical uncertainties (given in parentheses relative to the last digit of the mean) are one standard deviation.

N	P	h/t_0	t_f/h	ω	θ	N_t	ν	pV/Nk_BT	$\hat{D}(\theta h/t_0;N)$	$10^4 v_0$
108	22	0.0020	8000	2	826	176 000	21	4.155(105)	0.0438(18)	7.6
500	28	0.0020	8000	2	826	224 000	27	4.579(058)	0.0524(07)	3.3
864	5	0.0020	8000	4	828	40 000	3	4.320(043)	0.0512(11)	2.1
1372	27	0.0020	8000	4	828	216 000	24	4.355(023)	0.0516(03)	1.7

The time constant for $N=500$ is the largest of the three. Thus, we believe that the anomalous collision rate, which reflects the anomalous equation of state, is also the cause of the anomalous diffusion constant.

In order to demonstrate the long-time contributions to the VACF, we also plot in Fig. 3 the long-time tail, Eq. (3), in which the theoretical coefficient is given by[8,9]

$$\alpha_D=(2/3n\beta m)[4\pi(D+\eta/nm)t_0]^{-3/2}\,, \tag{39}$$

in which η is the shear viscosity coefficient. The evaluation shown in the figure is based on using the Levesque-Verlet[21] value $\hat{D}=0.054$ and the Levesque *et al.*[28] value $\hat{\eta}=4.0$. Evidently, the theoretical long-time tail fits onto the $N=1372$ VACF rather well. Integration of theoretical tail from $t/t_0=\theta\hat{h}=1.656$ to infinite time yields the tail contribution $\hat{D}_{\rm tail}=0.0028$.

For comparison with our values of $\hat{D}$, we recall the value $\hat{D}=0.054\pm0.003$ reported by Levesque and Verlet[21] for 864 particles, obtained by a Green-Kubo calculation in the molecular-dynamics ensemble. Because of the relatively large value of N, we expect any ensemble differences to lie well within the rather large statistical uncertainty. On the face of it, that value would appear to be in reasonable agreement with ours. Nonetheless, the details of their calculation are not entirely clear, and, in Fig. 3, the velocity autocorrelation function is distinctly negative at the longest time for which those authors discuss that function, viz., $\hat{t}=0.55$; see Fig. 3. On that basis, we would agree with Evans *et al.*[13] that the Levesque-Verlet value is an overestimate of the long-time limit. However, since Levesque and Verlet do not actually state what values of the time were used in obtaining their reported values of the diffusion constant, it is not possible to assess whether the apparent agreement might be to some extent fortuitous.

To complete the Green-Kubo calculation of the self-diffusion constant, we extrapolate our $N=500$, 874, and 1372 results for $\hat{D}(\theta\hat{h},N)$ using least squares (weighted by the inverse of the variances of the three points, Table I) to get an infinite-system estimate $\hat{D}(\theta\hat{h})=0.0511\pm0.0006$. We add to this the long-time tail contribution, obtaining $\hat{D}_{\rm GK}=0.0539\pm0.0006$.

B. Nonequilibrium molecular-dynamics results

The systems studied by NEMD are listed in Table II. The tabulated values of the diffusion constant include values both from the "driving" term, Eq. (17), labeled $\hat{D}_d$, and from the thermostat, Eq. (18), labeled $\hat{D}_s$. We observe that the former provide a somewhat more precise estimate for $\hat{D}$ at small values of the diffusion current density.

It should be noted from Table II that rather large values of Θ were used in the data analysis for the larger values of $\hat{J}_x$ in order to eliminate what appear to be long-lived transients, as discussed in Sec. III. For the most part, a coarse-graining interval Ω of about 5000 to 15 000 time step was used. For small $\hat{J}_x$, somewhat larger values of Ω were needed to eliminate the strong serial correlations. Indeed, it is by no means certain that a true steady state, rather than an oscillatory motion, underlies the observations. There would appear to be no way to prove numerically the existence of a low-level oscillation in the presence of slowly damped, random fluctuations. We have therefore been content to use these large coarse-graining intervals in treating the small $\hat{J}_x$ data.

1. Dependence of $\hat{D}$ on $\hat{J}_x$

The results for $\hat{D}_d$ are plotted as a function of $\hat{J}_x$ in Fig. 4, which also includes the Green-Kubo values at $\hat{J}_x=0$. For comparison, we have also included in Fig. 4 three of the "Gaussian algorithm" results of Evans *et al.* (for $N=108$) read from the figure in Ref. 13, assuming that the abscissa in that figure should contain the product of the number of particles and the current density J_x in place of the current I. Because the Evans *et al.* calculations extended to only 15 000 time steps, the uncertainties in their results are presumably somewhat larger than ours, but we have made no attempt to assign them values. The apparent agreement with our results confirms that the ef-

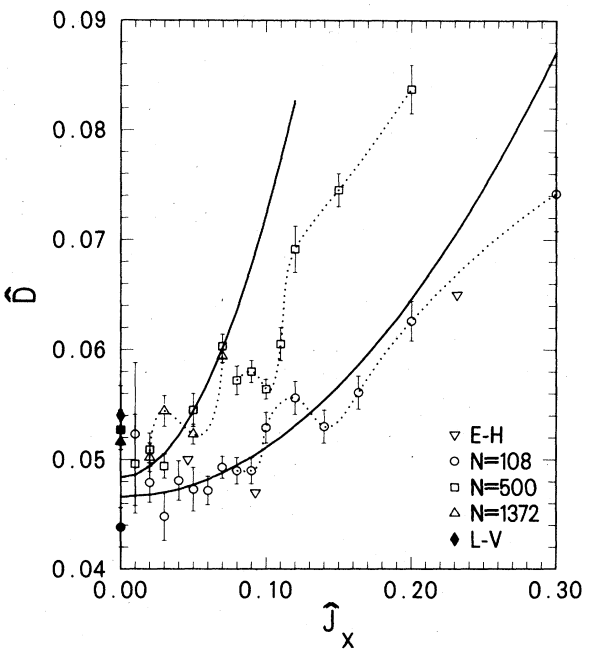

FIG. 4. Reduced diffusion constant $\hat{D}$ as a function of the reduced diffusion current density $\hat{J}_x$ as determined by the synthetic NEMD method (open symbols) for systems of 108 (circles), 500 (squares), and 1372 (triangles) Lennard-Jones particles, at a reduced density $\hat{n}=0.85$ and a reduced temperature $\hat{T}=1.08$. The three points (inverted triangles) are taken from Ref. 13 (EH). Green-Kubo values (solid symbols), plotted at $\hat{J}_x=0$, were determined both in this study (for 108, 500, and 1372 particles) and earlier, by Levesque and Verlet (LV) for $N=864$ (diamond). The solid curves are the regression curves, Eq. (40), for the 108- and 500-particles NEMD results. The dotted lines connect successive points with increasing $\hat{J}_x$ for each value of N only as a guide to the eye.

TABLE II. Parameters and results for the nonequilibrium molecular-dynamics calculation of the self-diffusion constant of the Lennard-Jones fluid at a reduced density $\hat{n}=0.85$ and reduced temperature $\hat{T}=1.08$. N is the number of particles, $\hat{J}_x$ is the reduced diffusion-current density, h is the integration time step, and Γ, Θ, and Ω specify the coarse graining used to obtain the steady-state diffusion constants, $\hat{D}_s$, Eq. (18), and $\hat{D}_d$, Eq. (17). N_t is the total number of time steps taken for the trajectory, ν is the number of degrees of freedom in the steady-state averages of the diffusion constants. The statistical uncertainties (given in parentheses relative to the last digit of the mean) are one standard deviation.

N	$\hat{J}_x$	h/t_0	Γ	Θ	Ω	N_t	ν	$\hat{D}_s$	$\hat{D}_d$
108	0.01	0.0020	6000	6000	17000	346000	19	0.0576(278)	0.0523(065)
	0.02	0.0020	6000	6000	23000	466000	19	0.0475(043)	0.0479(018)
	0.03	0.0020	6000	6000	5000	56000	9	0.0481(111)	0.0478(056)
	0.03	0.0020	6000	6000	10000	256000	24	0.0453(036)	0.0448(022)
	0.04	0.0020	6000	6000	5000	156000	29	0.0471(041)	0.0481(018)
	0.05	0.0020	6000	6000	10000	156000	14	0.0469(020)	0.0473(020)
	0.06	0.0020	6000	6000	5000	206000	39	0.0469(018)	0.0472(013)
	0.07	0.0020	6000	6000	5000	236000	45	0.0493(014)	0.0493(010)
	0.08	0.0020	6000	11000	5000	101000	17	0.0492(016)	0.0490(012)
	0.09	0.0020	6000	16000	5000	156000	27	0.0489(014)	0.0490(012)
	0.10	0.0020	0	10000	10000	170000	15	0.0528(016)	0.0529(014)
	0.12	0.0020	6000	31000	10000	151000	11	0.0554(014)	0.0556(015)
	0.14	0.0020	6000	6000	5000	86000	15	0.0529(015)	0.0530(015)
	0.20	0.0020	6000	36000	5000	106000	13	0.0660(021)	0.0648(018)
	0.30	0.0020	6000	26000	5000	56000	5	0.0739(033)	0.0742(034)
500	0.01	0.0020	0	5000	10000	125000	5	0.0470(200)	0.0496(035)
	0.02	0.0020	2000	12000	20000	152000	6	0.0511(022)	0.0509(009)
	0.03	0.0015	0	5000	5000	60000	10	0.0446(036)	0.0465(017)
	0.03	0.0020	2000	7000	10000	167000	15	0.0495(016)	0.0494(011)
	0.05	0.0015	6000	16000	15000	106000	5	0.0551(018)	0.0545(015)
	0.07	0.0015	6000	31000	5000	106000	24	0.0600(024)	0.0603(011)
	0.08	0.0020	0	5000	10000	45000	3	0.0572(020)	0.0572(011)
	0.09	0.0015	6000	33000	5000	86000	10	0.0580(008)	0.0580(010)
	0.10	0.0015	6000	6000	15000	156000	9	0.0564(010)	0.0564(009)
	0.10	0.0015	6000	6000	1000	16000	9	0.0557(038)	0.0567(020)
	0.11	0.0015	6000	26000	5000	116000	17	0.0605(016)	0.0605(015)
	0.12	0.0020	0	25000	10000	105000	7	0.0690(020)	0.0691(021)
	0.15	0.0015	6000	26000	5000	56000	9	0.0745(020)	0.0745(015)
	0.20	0.0015	6000	31000	5000	56000	4	0.0840(022)	0.0837(022)
1372	0.02	0.0020	0	7000	10000	77000	6	0.0523(031)	0.0502(013)
	0.03	0.0020	0	8000	8000	72000	7	0.0544(030)	0.0544(014)
	0.05	0.0020	0	6000	9000	51000	4	0.0525(019)	0.0523(009)
	0.07	0.0020	0	15000	5000	65000	9	0.0596(010)	0.0594(006)

fects of both the flow transients and differences in interaction potentials on the calculation of the diffusion constant are small.

In considering the data in Fig. 4, one feature seems to stand out particularly: With increasing $\hat{J}_x$, there are intervals for which the dependence of $\hat{D}_d$ on $\hat{J}_x$ changes rather abruptly. For $N=500$ especially, a rather sharp dip is seen to the right of $\hat{J}_x=0.07$. (Other instances of similar "structure" can be seen in the figure, but for $N=108$ these are of marginal statistical significance.) One might suppose this behavior to reflect structural changes in the fluid, induced by the driving force, reminiscent of the shear-induced ordering transition seen in the dense hard-sphere fluid,[29] as well as related phenomena seen in the soft-sphere fluid.[30] We have, therefore, computed the (transverse) Fourier components of the color density fluctuations, Eq. (36), in order to look for the onset of a secondary flow in the system. In Fig. 5, we plot the $F(1)$ for each of the system sizes as a function of the diffusion current $\hat{J}_x$. For $N=108$, this function seems to increase gradually and smoothly from the equilibrium value, Eq. (35), within its large statistical uncertainties, at least up to $\hat{J}_x=0.14$. While the pair correlation function in the direction transverse to the diffusion current evidently becomes increasingly unequal between the "like" and "unlike" particles, no sharp change in structure can be seen.

Unfortunately, the $N=500$ runs did not include the calculation of the structure factor for every value of $\hat{J}_x$ so that the interpretation of Fig. 5 is hampered somewhat by the lack of detail. However, by virtue of the smaller error bars for this case, we identify a rather sharp increase in $F(1)$ between $\hat{J}_x=0.08$ and 0.12. Indeed, at $\hat{J}_x=0.08$, $F(1)$ is double its equilibrium value. There would appear

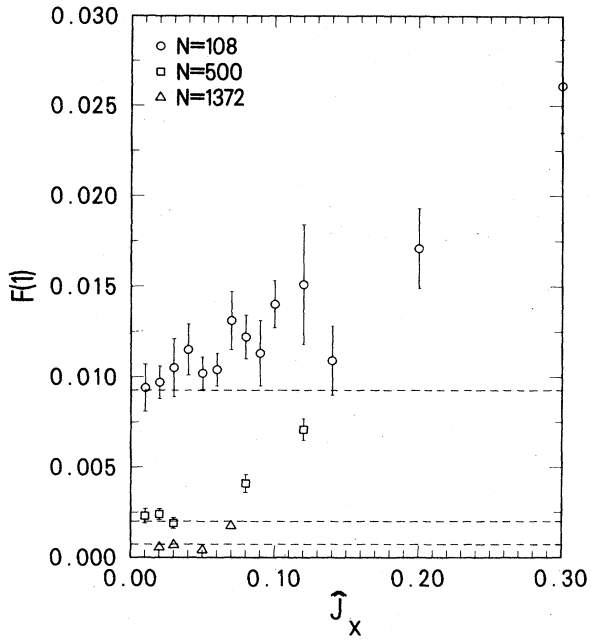

FIG. 5. Transverse, $k=1$, wave-number component of the mean fluctuation $F(1)$, Eq. (36), of the "color" density as a function of the reduced diffusion current $\hat{J}_x$ for NEMD calculations for 108 (circles), 500 (squares), and 1372 (triangles) Lennard-Jones particles at a reduced number density $\hat{n}=0.85$ and a reduced temperature $\hat{T}=1.08$. The equilibrium fluctuations are equal to $1/N$, and given by the horizontal broken lines. The error bars represent one standard deviation. The values of $F(1)$ have increased significantly at the largest values of the current plotted, indicating the possible presence of a secondary flow.

to be some suggestion that the homogeneous steady flow might have gone over into some sort of secondary flow involving a nonuniform color density. A definitive resolution of this possibility must await a more detailed study of the flow. For $N=1372$, similar observations apply, with a marked increase in $F(1)$ seen between $\hat{J}_x=0.05$ and 0.07.

2. *Extrapolation to $\hat{J}_x=0$*

A second observation suggested by Fig. 4, especially for $N=108$, is that the slope of the $D(J_x)$ function vanishes as J_x approaches zero. This behavior is consistent with the expectation that the diffusion constant should be an even function of the diffusion current; a change of sign of J_x must leave D unaffected. However, it contrasts with the work of Evans *et al.*,[13] who used a linear fit to extrapolate to $\hat{J}_x=0$. In the absence of evidence, either theoretical or numerical, to suggest some sort of singularity in this function, we see little justification for including a linear term in the fit and we have not done so.

To obtain a zero-diffusion-current value for the diffusion constant, we make a linear least-squares fit, weighted by the reciprocal of the square of the standard deviation $s(\hat{J}_x,N)$, as reported in Table II,

$$\hat{D}(\hat{J}_x;N)=\hat{D}_0(N)+\hat{D}_1(N)\hat{J}_x^2 \tag{40}$$

including the data up a number of different values of the maximum $\hat{J}_x^*$ guided somewhat by the results in Fig. 5. In Table III we list the results of the fits, for the three system sizes, for several different values of $\hat{J}_x^*$. The table includes approximate values for the goodness-of-fit parameter χ^2 evaluated as

$$\chi^2(\hat{J}_x^*,N)=\sum_{\hat{J}_x\le\hat{J}_x^*}\frac{[\hat{D}_d(\hat{J}_x,N)-\hat{D}^{\,\mathrm{ls}}(\hat{J}_x,N)]^2}{s^2(\hat{J}_x,N)} \tag{41}$$

in which $\hat{D}^{\,\mathrm{ls}}$ is the least-squares fit, listed in Table III. Except for $N=500$, $\hat{J}_x^*=0.2$, and $N=1372$, $\hat{J}_x^*=0.07$ the values of χ^2 are not exceptional. For $N=108$, the choice of $\hat{J}_x^*$ does not greatly affect the values of $\hat{D}_0$. For all three system sizes, we therefore use the second table entry as the NEMD result of choice.

We observe that the $N=108$ and 500 NEMD values are in reasonable statistical agreement, both between themselves and with the $\hat{J}_x=0$ extrapolation of the Evans *et al.*,[13] data given by Evans and Morriss,[31] viz., $\hat{D}=0.045\pm0.0025$. This result supports to a certain extent the contention that the NEMD method yields a

TABLE III. Results for the least-squares fit of the NEMD calculations of the self-diffusion constant for the reduced temperature and density $\hat{T}=1.08$, $\hat{n}=0.85$ to the form, Eq. (40). N is the number of particles, $\hat{J}_x^*$ is the largest value of the diffusion current density included in the fit, $\hat{D}_0$ and $\hat{D}_1$ are the regression coefficients, with one standard deviation uncertainties, ν is the number of degrees of freedom, χ^2 is the approximate goodness-of-fit parameter, Eq. (41), N_t is the total number of time steps for the runs used in the regression analysis, and v_0 is a normalized standard deviation for $\hat{D}_0$.

N	$\hat{J}_x^*$	$\hat{D}_0$	$\hat{D}_1$	ν	χ^2	N_t	$10^4 v_0$
108	0.30	0.0473(05)	0.36(03)	13	17.8	2 704 000	8.5
108	0.20	0.0466(06)	0.45(15)	12	11.6	2 648 000	9.4
108	0.12	0.0459(08)	0.60(12)	10	7.2	2 411 000	12.8
500	0.20	0.0504(05)	0.91(05)	11	69.4	1 336 000	5.6
500	0.07	0.0484(07)	2.38(29)	4	9.8	716 000	6.2
1372	0.07	0.0495(10)	1.94(25)	2	10.7	265 000	5.0
1372	0.05	0.0517(13)	0.35(69)	1	4.6	200 000	5.8

smaller N dependence than the Green-Kubo method, a matter to which we shall return below.

C. Relative efficiency of NEMD and Green-Kubo calculations

One of our goals was to evaluate the relative efficiency of the NEMD and the Green-Kubo calculations, both for a given value of N and in the thermodynamic limit. To set a numerical basis for comparison, we compute a "normalized" variance of the distribution from which the two methods obtain estimates of the diffusion constant, based on a fixed number of time steps in the molecular dynamics. In Tables I and III we give the number of time steps N_t which contribute to the final values of $\hat{D}$, along with the expected standard deviation v_0 for a calculation of 10^6 time steps. In both cases, we obtain v_0 by multiplying the standard deviation by the square root of $10^{-6}N_t$. We observe that the ratio of standard deviations for the NEMD calculation to the Green-Kubo calculation varies from 1.1 to more than 2.0. In making this comparison, we are aware, of course, that the precise values obtained for v_0 for the NEMD calculations are somewhat dependent on the extent of the calculations made at the various values of $\hat{J}_x$, but effects of this kind are very small. In particular, the NEMD error estimates are not inflated by the inclusion of the small J_x results, even though the latter tend to require larger numbers of time steps to achieve a fixed degree of precision.

The significance of the differences in v_0 between the Green-Kubo and the NEMD methods is a little difficult to assess. For the numbers of degrees of freedom ν, for Tables I and III, the standard F test[24] for comparing variances finds the $N=108$ variance ratio of 1.3 (NEMD to Green-Kubo, using the $\hat{J}_x^*=0.3$ value from Table III) to be significant only at (roughly) the 70 percent level. The $N=500$ ratio (using the $\hat{J}_x^*=0.07$ value from Table III) of 5.4 is significant at about the 99.5 percent level (even though the NEMD result contains only 4 degrees of freedom). For $N=1372$, the ratio of 11.4 (based on $\hat{J}_x^*=0.05$) is significant well above the 99.5 percent level. Moreover, were we to inflate the degrees of freedom for the NEMD calculations to include those of the underlying calculations from Table II, the level of significance for these ratios would be even higher. If, on the other hand, we use the larger values for $\hat{J}_x^*$ for $N=500$ and 1372, the ratios remain large and quite significant. Clearly, our results show the Green-Kubo calculations to be advantageous, particularly for the larger system sizes for which the results for large J_x cannot be used in the estimation of $\hat{D}$ because of the presence of the changing functional form of $\hat{D}(\hat{J}_x,N)$. In this connection, we point out that, if we limit the range of $\hat{J}_x$ in the least-squares fit for $N=108$, as in the third line of Table III, the normalized error increases dramatically. It appears, therefore, that the NEMD calculation loses much of its power to evaluate $\hat{D}_0$ as the range of the current is limited.

D. Comparison of Green-Kubo and NEMD self-diffusion constants: N dependence

We noted above that the NEMD method seems to yield values of the transport coefficient which, on the basis of the 108- and 500-particle results, might be interpreted as independent of N. The extent to which this is true can be seen graphically in Fig. 6 in which all of the values for the self-diffusion constant at $\hat{J}_x=0$ are plotted as a function of $1/N$, including the Evans-Morriss extrapolation.[31] If we were to ignore the $N=1372$ NEMD point, one would conclude that the $N=108$ and 500 imply an infinite-system result ($\hat{D}=0.0489\pm0.0009$) which would be in clear conflict with the Green-Kubo results. The latter are shown by the dash-dot line in the figure, which is the least-squares fit for $\hat{D}(\theta\hat{h},N)$, discussed above. Inclusion of the long-time tail contribution yields the point marked

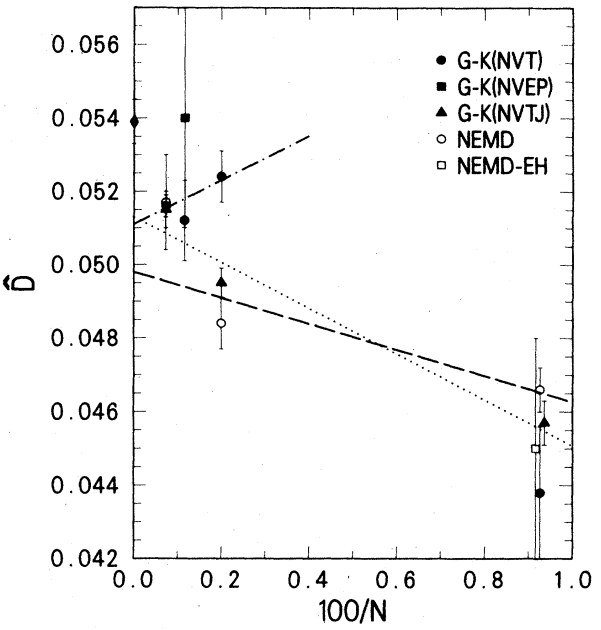

FIG. 6. Reduced diffusion constant $\hat{D}$ from Green-Kubo (filled symbols) and from NEMD calculations (open symbols) as a function of the reciprocal of the number of particles N. The errors bars represent one standard deviation. The values at $N=108$ have been displaced slightly either to the left or the right in order to facilitate distinguishing the points. The circles and triangles are results from the present study, the squares are earlier results, including the Green-Kubo result of Levesque and Verlet for the molecular-dynamics (N-V-E-P) ensemble and the NEMD result (EH) of Evans *et al.* The Green-Kubo results are the values of $\hat{D}(\theta\hat{h};N)$ and do not include the long-time tail (for times beyond θh). The dash-dotted line shows the least-squares fit for the N-V-T ensemble data for $N\geq500$. The diamond symbol at $1/N=0$ marks the complete N-V-T ensemble result, including the theoretical long-time tail. The dashed line is the least-squares fit of the three NEMD data points (open circles) determined in the present work. The dotted line is the least-squares fit to the N-V-T-J ensemble Green-Kubo results (solid triangles).

by a diamond in the figure. While it is possible that $N=500$ is not sufficiently large for the (Green-Kubo) $1/N$ extrapolation to be valid, this seems unlikely in view of hard-sphere equation of state study[26] in which $N=500$ clearly was in the $1/N$ regime. Moreover, the $N=864$ result, while not nearly as precise as the other values, is also consistent with this view.

A more likely explanation of the discrepancy between the Green-Kubo and NEMD results is provided by the $N=1372$ NEMD point which suggests, despite its large error bar, that the N dependence of the NEMD calculation becomes stronger at large N, and is in the opposite direction to that of the Green-Kubo results. A least squares fit of all three NEMD values yields $\hat{D}=0.0498\pm0.0008$, shown by the dashed line in Fig. 6. This result continues to disagree with the Green-Kubo value. On the other hand, extrapolation of the values for the two larger systems yields $\hat{D}=0.0536\pm0.0021$ which is in agreement with the Green-Kubo value. It seems likely, then, that the 108-particle NEMD system is also anomalous with respect to N dependence, but the effect is smaller than for the N-V-T ensemble Green-Kubo calculation.

E. Green-Kubo results for N-V-T-J ensemble

To shed further light on this subject, we have also performed an additional set of Green-Kubo calculations, but using an ensemble more closely tied to the NEMD calculations. We define the N-V-T-J ensemble to have fixed values of both the diffusion current $J_x=0$ and the transverse kinetic energy E_t, just as in the NEMD calculations. The y and z components of diffusion current as well as the x component of kinetic energy fluctuate as in the canonical ensemble.

Dynamically, we use the NEMD equations of motion so that J_x and E_t remain fixed. Because of the λ_s term in the equations of motion, the Liouville theorem does not hold for the system. Nonetheless, the calculations were done using the NEMD equations of motion in the expectation that the NEMD calculations might approach them in the limit of vanishing diffusion current. We have not proved this and present the results as an interesting sidelight.

Calculations in this ensemble are entirely analogous to those in the canonical ensemble. Now, however, in order to set the initial value of the diffusion current to zero, we subject the x components of the Monte Carlo velocities produced by the Box-Muller method to a rotation about the origin onto the $J_x=0$ hyperplane, viz.,

$$
\begin{aligned}
v'_{x,2i+1} &= \frac{L_1+L_2}{\sqrt{2}L}v_{x,2i+1}-\frac{L_1-L_2}{\sqrt{2}L}v_{x,2i+2}\,,\\
v'_{x,2i} &= \frac{L_1-L_2}{\sqrt{2}L}v_{x,2i-1}+\frac{L_1+L_2}{\sqrt{2}L}v_{x,2i}\,,\\
L^2 &= L_1^2+L_2^2\,,
\end{aligned}
\tag{42}
$$

in which the L_i are given in Eq. (16). The y and z components of velocity are projected onto the surface of fixed transverse energy.

The results of these calculations are shown in Table IV and Fig. 6. We note that the N dependence of the diffusion constant is opposite in sign to that in the N-V-T ensemble. While the compressibility factor does not appear to be monotonic in N, the 108-particle value does not lie nearly so far from the line formed by the 500- and 1372-particle values as was the case for the canonical ensemble. Similarly, the 108-particle diffusion constant is not nearly so far out of line with the larger system results. Moreover, the values of the $\hat{D}(\theta\hat{h},N)$ are quite consistent with the ($\hat{J}_x=0$) extrapolated NEMD results. Because of the relatively high precision of the values of $\hat{D}(\theta\hat{h},N)$ for this ensemble, especially for $N=1372$, the value of D obtained by extrapolating the values for all three systems to the thermodynamic limit, viz., $\hat{D}(\theta\hat{h})=0.0513\pm0.0004$ (shown by the dotted line in Fig. 6), now agrees with the N-V-T ensemble Green-Kubo value. The extrapolation of the $N=500$ and 1372 results, $\hat{D}(\theta\hat{h})=0.0526\pm0.0008$, while somewhat larger than the N-V-T ensemble result, nevertheless remains in statistical agreement.

We conclude, therefore, that the N dependence of the NEMD calculation is no less than that of the Green-Kubo method. Moreover, it appears that $N=108$ is too small a value, at least at the present high density, to permit a $1/N$ extrapolation, just as it is with the Green-Kubo method (at least in the N-V-T ensemble). Perhaps most interesting is the difficulty one encounters in finding the correct N dependence of the NEMD results. This arises because the dependence of D on the diffusion current becomes increasingly complicated as J_x increases, perhaps because the homogeneous flow becomes unstable, and the value of J_x at which this complication arises decreases with increasing N. Thus, the range of useful values of the diffusion current for the NEMD calculations becomes limited to such small values that the statistical uncertainties far exceed those for the Green-Kubo method.

V. DISCUSSION

We would like to stress the following points in connection with the calculations reported here.

TABLE IV. Parameters and results for the Green-Kubo calculations of the self-diffusion constant for the Lennard-Jones fluid in the N-V-T-J ensemble at a reduced density $\hat{n}=0.85$ and reduced temperature $\hat{T}=1.08$. See Table I for symbols.

N	P	h/t_0	t_f/h	ω	θ	N_t	pV/Nk_BT	$\hat{D}(\theta h/t_0;N)$	10^4v_0
108	26	0.0020	8000	2	826	208 000	4.308(13)	0.0457(06)	2.7
500	10	0.0020	8000	2	826	80 000	4.393(17)	0.0495(04)	1.1
1372	6	0.0020	8000	4	828	48 000	4.366(20)	0.0515(05)	1.1

(i) As discussed in part in the introduction, the goal of NEMD is the study of nonequilibrium processes, both in the so-called linear limit, in which the hydrodynamic currents are linear in the gradients, as well as far from equilibrium. While our critique has been limited to the use of NEMD in the first of these areas, viz., the evaluation of the Fick's law self-diffusion constant, it is worthwhile to realize that self-diffusion provides a particularly important test for the "far from equilibrium" applications as well. In particular, because the self-diffusion current is linear in the concentration gradient irrespective of the magnitude of the gradient, a NEMD method generally suitable for self-diffusion should retain this property.

In the present synthetic NEMD algorithm, there is no concentration gradient. Nonetheless, in order to correctly account for self-diffusion, the diffusion constant should be independent of the diffusion current. Evidently, the present NEMD method does not meet this criterion.

(ii) Within the context set out in the introduction, viz., the comparison of the Green-Kubo method with synthetic NEMD method in the evaluation of linear transport coefficients, our calculations have demonstrated rather unambiguously the superiority of Green-Kubo, at least within the limitations of the present NEMD calculations, viz., the use of the Gaussian algorithm (rather than, say, constant driving force) with the thermostat applied to only the transverse velocity components (rather than all three components of velocity). It seems unlikely that simple variations of the method would materially affect the results. The reasons for the superiority of the Green-Kubo method are of considerable interest in assessing future developments in this field.

(iii) The present NEMD method fails to effectively provide the correct dependence of the diffusion constant on the size of the system. Indeed, at first sight, we seemed to find a transport coefficient which is independent of N, just as reported in the literature. Only when we extended our calculations to sufficiently high accuracy were we able to see that the assumption of N independence yielded results in conflict with the Green-Kubo results. It was then necessary to extend the NEMD calculations to $N=1372$ in order to resolve the disagreement and find the correct dependence on N.

(iv) Because the statistical uncertainties are typically large in the numerical calculation of transport coefficients and because the N dependence of transport coefficients is not particularly large, the conclusion reached in previous studies, viz., that NEMD calculations have small N dependence but agree with Green-Kubo calculations, is understandable. The present choice of self-diffusion, rather than shear viscosity or thermal conductivity, as a test case, permits the precision of the calculations to be improved considerably.

(v) The difficulty in obtaining the correct N dependence for NEMD calculations is largely psychological rather than real. For example, one does not do NEMD calculations at values of the current sensibly smaller than those used here because the signal-to-noise ratio becomes too small. Indeed, for $N=108$, the variance of the diffusion constant for the Green-Kubo method is smaller than for the NEMD method for $\hat{J}_x$ below about 0.05. If the practitioner is forced (by other circumstances) to do calculations at much smaller values of the current, the realization that the Green-Kubo method is more "efficient" would normally dissuade the investigation of these small currents.

(vi) In the present calculations, the circumstance which forces the investigation of small currents is the apparent presence of hydrodynamic instabilities in the homogeneous fixed-current diffusive flow. In our calculations, we have certainly not established the existence of secondary flows, even though our calculations of the color density fluctuations strongly suggest it. Moreover, to simply pretend that the flow remains homogeneous leads to even more serious disagreement with the Green-Kubo results. Because the supposed instability arises at smaller values of $\hat{J}_x$ as N increases, for N as small as 1372 the largest "stable" value of the reduced current is at most only 0.05. Calculations for smaller values of the current for this system size are found to be much more expensive in computer time than the Green-Kubo calculations.

While one would certainly expect the detailed behavior we have reported here to be peculiar to the self-diffusion problem, there is every reason to believe the conclusions to have general applicability for any transport property. The fact that shear viscosity has apparently been treated successfully through NEMD probably reflects the lack of a truly critical comparison between Green-Kubo and NEMD, arising at least in part from the generally larger statistical uncertainties for viscosity compared to self-diffusion for equal amounts of computing effort. Moreover, at least in one case,[27] there exist evidence for disagreement between Green-Kubo and NEMD which has not, to our knowledge, been satisfactorily explained. We note, however, that the present NEMD method for self-diffusion seems not to truly reflect the self-diffusion process. In particular, the Green-Kubo calculation takes advantage of the fact that a single-phase-space trajectory provides N distinct (but not necessarily independent) measures of the self-diffusion time-correlation functions. It is by no means evident that the current NEMD algorithm similarly reflects the nature of self-diffusion. As a result, we believe it to be entirely possible that the large statistical advantage we see here for the Green-Kubo method might well be special to self-diffusion.

(viii) The reader should notice the highly significant improvement in the precision of the values of the self-diffusion constant for the N-V-T-J ensemble, using the NEMD equations of motion, over the N-V-T ensemble, as shown by a comparison of the values of v_0 in Tables I and IV. The N-V-T ensemble appears to be a particularly poor choice with respect to these calculations; the so-called molecular-dynamics ensemble (the microcanonical ensemble, but with fixed total momentum) is typically a better choice because of the absence of fluctuations in the center of mass velocity. Nonetheless, we believe it unlikely the molecular-dynamics ensemble would yield such a large statistical improvement. Rather, the non-Hamiltonian terms in the equations of motion (leading to conservation of transverse kinetic energy and diffusion current) would appear more likely to be the source of the

improvement. In addition to an understanding of why this is so, a justification for this variant of the Green-Kubo method would most certainly be of value.

ACKNOWLEDGMENTS

The author is grateful to W. W. Wood of Carroll College, E. G. D. Cohen of The Rockefeller University, P. B. Visscher of the University of Alabama, and B. L. Holian of this laboratory for a number of discussions. This work was supported by the U.S. Department of Energy (Division of Chemical Sciences, Office of Basic Energy Sciences).

[1]B. J. Alder and T. Wainwright, *International Symposium on Statistical Mechanical Theory of Transport Properties, Brussels, 1956,* edited by I. Prigogine (Interscience, New York, 1958).

[2]M. S. Green, J. Chem. Phys. **20**, 1281 (1952); **22**, 398 (1954).

[3]R. Kubo, J. Phys. Soc. Jpn. **12**, 570 (1957).

[4]J. J. Erpenbeck and W. W. Wood, in *Modern Theoretical Chemistry,* Vol. 6, Part B of *Statistical Mechanics, Time Dependent Processes,* edited by B. J. Berne (Plenum, New York, 1977).

[5]B. J. Alder and T. E. Wainwright, Phys. Rev. Lett. **18**, 988 (1967); Phys. Rev. A **1**, 18 (1970).

[6]J. J. Erpenbeck and W. W. Wood, Phys. Rev. A **26**, 1648 (1982).

[7]J. J. Erpenbeck and W. W. Wood, Phys. Rev. A **32**, 412 (1985).

[8]J. R. Dorfman and E. G. D. Cohen, Phys. Rev. Lett. **25**, 1257 (1970); Phys. Rev. A **6**, 776 (1972); **12**, 292 (1975).

[9]M. H. Ernst, E. H. Hauge, and J. M. J. van Leeuwen, Phys. Rev. Lett. **25**, 1254 (1970); Phys. Rev. A **4**, 2055 (1971); J. Stat. Phys. **15**, 7 (1976); **15**, 23 (1976).

[10]A. W. Lees and S. F. Edwards, J. Phys. C **5**, 1921 (1972).

[11]E. M. Gosling, I. R. McDonald, and K. Singer, Mol. Phys. **26**, 1475 (1973).

[12]W. T. Ashurst and W. G. Hoover, Phys. Rev. Lett. **31**, 206 (1973); Phys. Rev. A **11**, 658 (1975); W. G. Hoover and W. T. Ashurst, in *Theoretical Chemistry: Advances and Perspectives,* edited by H. Eyring and D. Henderson (Academic, New York, 1975), Vol. 1.

[13]D. J. Evans, W. G. Hoover, B. H. Failor, B. Moran, and A. J. C. Ladd, Phys. Rev. A **28**, 1016 (1983).

[14]D. J. Evans and G. P. Morriss, Comput. Phys. Rep. **1**, 6 (1984).

[15]D. J. Evans, in Proceedings of the 1985 Enrico Fermi School of Physics [Nuovo Cimento (to be published)].

[16]W. G. Hoover, Ann. Rev. Phys. Chem. **34**, 103 (1983); Phys. Today **37**, 44 (1984).

[17]W. W. Wood and J. J. Erpenbeck, J. Stat. Phys. **27**, 37 (1982).

[18]B. L. Holian and D. J. Evans, J. Chem. Phys. **78**, 5147 (1983).

[19]W. W. Wood, in *Physics of Simple Fluids,* edited by H. N. V. Temperley, J. S. Rowlinson, and G. S. Rushbrooke (North-Holland, Amsterdam, 1968).

[20]B. Jansson, *Random Number Generators* (Pettersons, Stockholm, 1966).

[21]D. Levesque and L. Verlet, Phys. Rev. A **2**, 2514 (1970).

[22]B. J. Berne and G. D. Harp, in *Advances in Chemical Physics* (Interscience, New York, 1973), Vol. XVII.

[23]L. Verlet, Phys. Rev. **159**, 98 (1967).

[24]A. Hald, *Statistical Theory With Engineering Applications* (Wiley, New York, 1952).

[25]W. W. Wood, J. Chem. Phys. **48**, 415 (1968); **52**, 729 (1970).

[26]J. J. Erpenbeck and W. W. Wood, J. Stat. Phys. **35**, 321 (1984).

[27]W. G. Hoover, D. J. Evans, R. B. Hickman, A. J. C. Ladd, W. T. Ashurst, and B. Moran, Phys. Rev. A **22**, 1690 (1980).

[28]D. Levesque, L. Verlet, and J. Kurkijarvi, Phys. Rev. A **7**, 1690 (1973).

[29]J. J. Erpenbeck, Phys. Rev. Lett. **52**, 1333 (1984).

[30]L. V. Woodcock, Chem. Phys. Lett. **111**, 455 (1984).

[31]D. J. Evans and G. P. Morriss, Phys. Rev. A **31**, 3817 (1985).